Journal of Sustainability Science and Management Special Issue Number 2: Fundamental Interdisciplinary Pathways To Future Sustainability 2017: 49-57
ISSN: 1823-8556
© Penerbit UMT

STRUCTURAL AND LUMINESCENT DIVERSITIES OF Eu^{3+} ACTIVATED Gd_2O_3 NANOPHOSPHORS

OON JEW LEE[1*], NURUL NORFARINA HASBULLAH[1,2], HUI SAN LEE[1], SOO KIEN CHEN[2] AND ZAINAL ABIDIN TALIB[2]

[1]*School of Fundamental Science, Universiti Malaysia Terengganu, 21030 Kuala Nerus, Terengganu, Malaysia.*
[2]*Department of Physics, Faculty of Science, Universiti Putra Malaysia, 43400 Serdang, Selangor, Malaysia.*

**Corresponding author: oonjew@umt.edu.my*

Abstract: In this work, the synthesis of $Gd_2(OH)_3:Eu^{3+}$ nanowires via hydrothermal reaction at 200 °C and pH 12. Cubic $Gd_2O_3:Eu^{3+}$ nanowires with high aspect ratio of ~ 266.7 were formed after subsequent calcination of the as-synthesised hexagonal $Gd_2(OH)_3:Eu^{3+}$ at 750 °C. The cubic $Gd_2O_3:Eu^{3+}$ shows larger band gap than that of the as-synthesised $Gd_2(OH)_3:Eu^{3+}$ because of its reduced structural order-disorder. The origin of the dominant red emission for $^5D_0$ - $^7F_2$ transition between the $Gd_2(OH)_3:Eu^{3+}$ and $Gd_2O_3:Eu^{3+}$ does not solely rely on the manifold *f-f* transitions of Eu^{3+} dopants but depends on the crystallographic symmetry and structural imperfection of Gd_2O_3 host.

Keywords: Photoluminescent, hydrothermal synthesis and nanowires

Introduction

The discovery of nanostructured rare-earth oxides has revolutionized related research on optoelectronic devices and biomolecule labelling due to their unique properties such as excellent photochemical stability, manifolds *f-f* transition and high refractive index ($n \sim 2$) (Guo *et al.*, 2004; Lee *et al.,* 2010; de Moura *et al*., 2014). In addition, the rare-earth oxides have been perceived as a prominent replacement for currently available fluorescent probes used in the fluorescent displays and magnetic resonance imaging (MRI) namely organic dyes, rare-earth doped oxysulfide, vanadates, ferrites and chelates (Jeong *et al.*, 2006; Goldys *et al.*, 2006; Shim *et al.*, 2007; Grandhe *et al.*, 2013).

However, all of the aforementioned materials exhibit low photothermal stability. Some of them (particularly oxysulfide and chelates) emit corrosive gas under electron bombardment (Rajan & Gopchandran, 2009). Furthermore, the high magnetic susceptibility of ferrites influences the MRI signal of neighbouring normal tissues, resulting in unclear images (Grandhe *et al.*, 2013). In order to mitigate the problems, cubic Eu-doped Gd_2O_3 (denoted as $Gd_2O_3:Eu^{3+}$) has been studied intensively due to its durable photothermal and chemical stability, narrow band gap and large Stokes shifts (Rajan & Gopchandran, 2009; Dhananjaya *et al.*, 2010). The excellent chemical stability characteristics of $Gd_2O_3:Eu^{3+}$ enable it to be adopted into the *in vivo* and *in vitro* biological labelling studies. The researchers also indicated the biocompatibility of $Gd_2O_3:Eu^{3+}$ where there is no signicant cytotoxic effect occuring inside the biological cells in long term (Luo *et al.*, 2014). Furthermore, there is a finding indicates that the Gd based compounds can be effectively removed by the wastewater treatment plants (Telgmann, *et al.*, 2013). Hence, we believe that $Gd_2O_3:Eu^{3+}$ would have low ecotoxicity and less environmental impact, leading towards environmental sustainability.

Of all rare-earth oxides, $Gd_2O_3:Eu^{3+}$ demonstrates tunability in luminescence properties by modifying its crystal structure, size and morphology (Lee *et al.*, 2010; Dhananjaya *et al.*, 2010). Knowing that the one-dimensional (1D) silicon nanowires exhibit superior luminescent and anti-reflection

performances (Yang *et al*., 2007; Lee *et al.*, 2010; Kiraly *et al*., 2013; Hazarika & Mohanta, 2016), the Gd_2O_3:Eu^{3+} nanowires might have the similar properties. The unique 1D nanostructure minimises the luminescent scattering and thus enhancing its luminescent intensity (Kiraly *et al.*, 2013). Nevertheless, synthesis of Gd_2O_3:Eu^{3+} phosphorous with controllable size and shape is still a challenge.

In this regard, hydrothermal method is a promising approach to synthesize isotropic and anisotropic Gd_2O_3:Eu^{3+} nanostructures compared with other synthesis routes like combustion, sol-gel, pyrolysis, precipitates and polyol chemical methods etc (Yang *et al.*, 2005; Goldys *et al.*, 2006; Lin *et al.*, 2007; Dhananjaya *et al.*, 2010; Maalej *et al.*, 2015). This route offers various advantages including simplicity, high yield and low cost in sample preparation (Lee *et al.*, 2008). It has been found that the synthesis temperature and pH are the key parameters which enable the diversity of nanostructures. As reported previously, 1D Gd_2O_3:Eu^{3+} nanowires can be obtained when the synthesis temperature was maintained at 180 °C while the pHs were regulated in the range of 11 – 12 (Lee *et al.*, 2008). Gd_2O_3:Eu^{3+} nanorods can be formed either at lower synthesis temperature of 145 °C in strong alkaline solution (pH 12) or at 180 - 200 °C in mild alkaline solution (pH 8 - 10) (Yang *et al.*, 2007; Lee *et al*., 2008; Dhananjaya *et al.*, 2010; Hazarika & Mohanta, 2016).

In this work, we focus on the hydrothermal synthesis of hexagonal $Gd_2(OH)_3$:Eu^{3+} at temperature 200 °C and pH 12 with longer synthesis duration (72 hours) as compared to the synthesis conditions reported in previous studies (Yang *et al.*, 2007; Lee *et al.*, 2008). We demonstrate the formation of cubic Gd_2O_3:Eu^{3+} 1D nanowires when the as-synthesised $Gd_2(OH)_3$:Eu^{3+} was subsequently underwent dehydration and calcination at 750 °C for 5 hours. The morphological evolution and luminescence features of the 1D Gd_2O_3:Eu^{3+} nanowires are discussed and highlighted.

Experimental

Gd_2O_3 and Eu_2O_3 with analytical grade of 99.99% and 99.90% purity; respectively, were used as starting powders to synthesize Gd_2O_3:Eu^{3+} using hydrothermal method. The stoichiometric amounts of Gd_2O_3 and 8 mol% Eu_2O_3 were dissolved in 1.0 M HNO_3 to form a clear solution. An aqueous 1.0 M NaOH was then added to adjust the pH of the solution to be in the range of alkaline (pH ~12) for the formation of colloidal hydroxide precipitates. The resulting precipitates were then loaded into a teflon-lined stainless steel autoclave to be placed into an oven which had been preset to 200 °C for 72 hours. The reaction product $Gd_2(OH)_3$: Eu^{3+} obtained in this way was washed with ethanol, collected through centrifugation and dried at 60 °C (hereafter denoted as as-synthesised $Gd_2(OH)_3$:Eu^{3+}) The $Gd_2(OH)_3$:Eu powder was calcined at 750 °C for 5 hours with the ramping rate of 3 °C/min in order to yield Gd_2O_3:Eu^{3+}. The phase and structural identification of the as-synthesised $Gd_2(OH)_3$:Eu^{3+} and Gd_2O_3:Eu^{3+} powders were performed by using the Rigaku Miniflex X-ray diffractometer with Cu Kα ranging from 20° to 80°. The nanostructural and surface morphology of the samples were imaged using a JEOL scanning electron microscope (SEM) operated at 15 kV. The samples were sputter-coated with a thin layer of Au before the imaging process was carried out. Measurements of UV-Vis absorption and photoluminescence emission spectra were performed at room temperature using Perkin Elmer Lambda 25 UV-vis spectrometer and Perkin Elmer LS 55 Fluorescence spectrometer; respectively. The UV-vis absorbance were obtained in the range of 200 nm - 900 nm. The photoluminescence emission spectra were measured at room temperature with Xenon flash lamp radiation in the range of 560-720 nm under the excitation wavelength of 257 nm

Result and Discussion

Figure 1 shows the X-ray diffraction (XRD)

patterns of the as-synthesised $Gd_2(OH)_3:Eu^{3+}$ and $Gd_2O_3:Eu^{3+}$ powders. The $Gd_2O_3:Eu^{3+}$ exhibits cubic phase with preferential orientation of (222) plane after calcination at 750 °C for 5 hours whereas the as-synthesised $Gd_2(OH)_3:Eu^{3+}$ forms hexagonal phase. No trace of Eu_2O_3 as secondary phase was observed in the XRD patterns of these two powders. The as-synthesised $Gd_2(OH)_3:Eu^{3+}$ and $Gd_2O_3:Eu^{3+}$ were indexed according to JCPDS file no. 83-2037 and 73-6280, respectively.

The lattice parameters and unit cell volumes were calculated according to the interplanar *d*-spacing equations for hexagonal and cubic structures, respectively (Cullity, 2001). The hexagonal $Gd_2(OH)_3:Eu^{3+}$ has a unit cell volume of 125.828(0) $Å^3$ with its lattice parameters $a = b = 6.316(7)$ Å and $c = 3.6413(8)$ Å. The cubic $Gd_2O_3:Eu^{3+}$ is under tensile strain due to doping as its lattice parameters and unit cell volume are expanded to $a = b = c = 10.810(3)$ Å and 1263.305(6) $Å^3$, respectively. For pure Gd_2O_3 with cubic crystal structure, its lattice parameters are $a = b = c = 10.790(0)$ Å. Such an expansion is evidenced by the marginal shifting of $Gd_2O_3:Eu^{3+}$ (222) peak towards lower angle in the XRD pattern (inset of Figure 1) in comparison with that of the pure Eu_2O_3 and Gd_2O_3. These observation indicates the doping effect of Eu^{3+} into the Gd_2O_3 structure when the smaller Gd^{3+} (ionic radius = 0.94 Å) is substituted by larger Eu^{3+} (ionic radius = 1.07 Å) (Shin *et al.*, 2005; Mukherjee *et al.*, 2009). In addition, the relatively narrower XRD peaks of $Gd_2O_3:Eu^{3+}$with full width at half maximum (FWHM) in the range of 0.31° – 0.36° suggest the highly crystalline nature of the $Gd_2O_3:Eu^{3+}$ in contrast to the as-synthesised $Gd_2(OH)_3:Eu^{3+}$ with higher FWHM of 0.43°-0.76°. The larger FWHMs of $Gd_2(OH)_3:Eu^{3+}$ is attributed to the higher degree of structural order-disorder in its lattices.

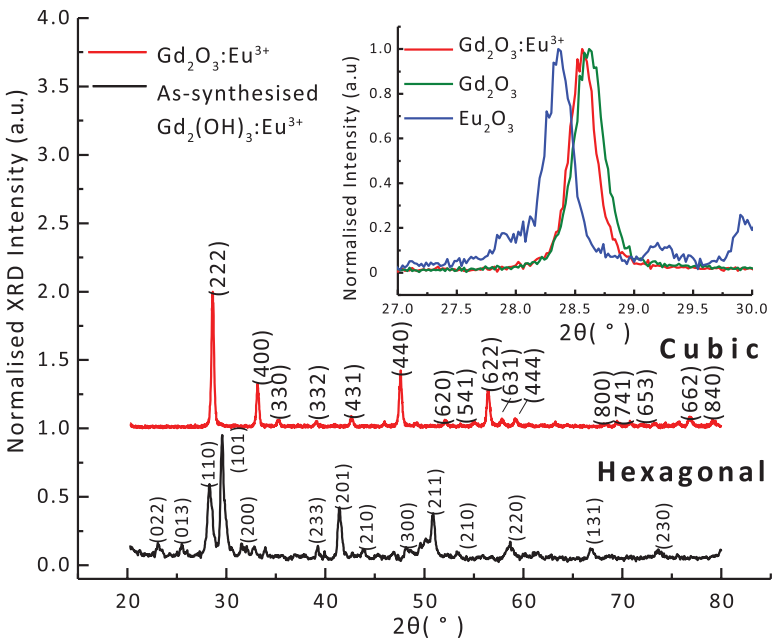


Figure 1: X-ray diffraction patterns of the as-synthesised $Gd_2(OH)_3:Eu^{3+}$ and $Gd_2O_3:Eu^{3+}$ nanophosphors. The inset shows the peak shifting of $Gd_2O_3:Eu^{3+}$ around (222) reflection as compared to pure Gd_2O_3 and Eu_2O_3

In order to obtain an insight into the morphology of the as-synthesised $Gd_2(OH)_3:Eu^{3+}$ and Gd_2O_3: Eu^{3+} nanostructures, their SEM images were captured and shown in Figure 2. The as-synthesised $Gd_2(OH)_3:Eu^{3+}$ appeared in the form of nanowires embedded within the randomly distributed two and three dimensional (2D and 3D) nanoflakes as shown in Figure 2 (a). The nanoflakes were grown from the $Gd_2(OH)_3:Eu^{3+}$ nuclei via 1D growth and subsequently agglomerated into 2D and 3D clusters. A similar 1D nucleation and growth was observed in ZnO synthesised by microwave-assisted hydrothermal method (Kharisov *et al.,* 2012). The 1D $Gd_2(OH)_3:Eu^{3+}$ nanowires shown in Figure 2 (b) have the average diameter of 30 nm and length of 200 nm that gives the aspect ratio (height/width) of 6.7. However, upon calcination at 750 °C the 1D nanowires elongated to ~ 8 µm in length whereas their diameters remained the same (Figure 2 (c)). The average length of these nanowires is about two times longer than that of the $Gd_2O_3:Eu^{3+}$ (2 - 3 µm in length) prepared by Lee *et al*. (2008) via hydrothermal reaction at 180 °C (Lee *et al*., 2008). It is noteworthy that similar pH 12 was used in this work and their studies (Lee *et al*., 2008). These calcined 1D nanowires possess a high aspect ratio of 266.7.

A key reason for this is that the surface energy along the preferential direction is lowered and thus assisting the elongation (Hazarika & Mohanta, 2016). Besides the elongation, the anisotropic distribution of these 1D nanowires was reduced considerably. Multiple $Gd_2O_3:Eu^{3+}$ nanowires rearranged themselves into arrays or bunch of nanowires, affirming the presence of 1D preferential growth. Both $Gd_2(OH)_3:Eu^{3+}$ and $Gd_2O_3:Eu^{3+}$ nanowires were relatively straight unlike the winding and curvy growth of $Gd_2O_3:Eu^{3+}$ nanotubes with the aid of multi

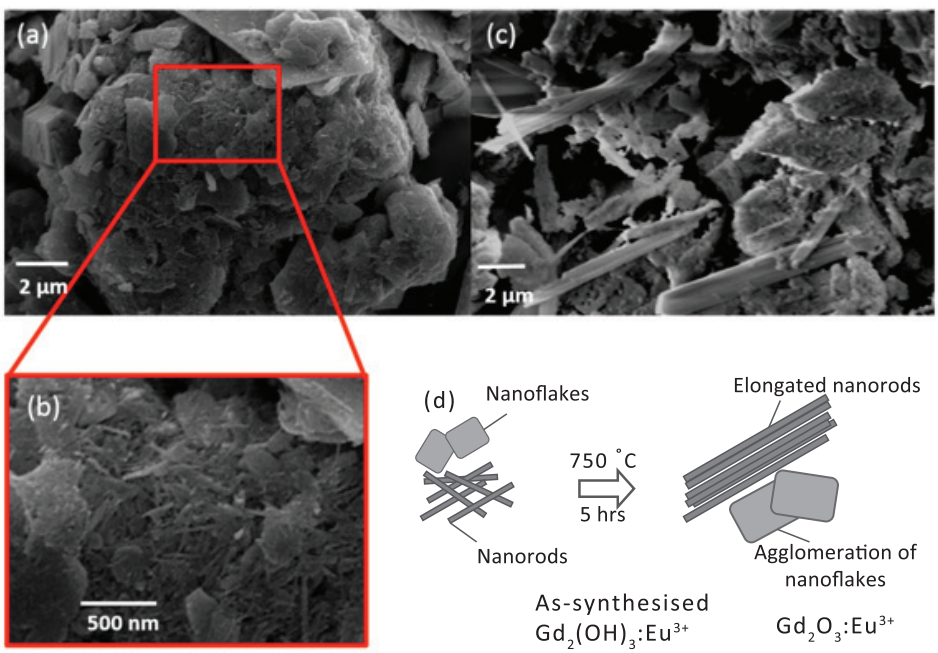


Figure 2: Structural morphology of the as-synthesised $Gd_2(OH)_3:Eu^{3+}$ and $Gd_2O_3:Eu^{3+}$ nanophosphors. (a) as-synthesised $Gd_2(OH)_3:Eu^{3+}$; (b) magnified image of $Gd_2(OH)_3:Eu^{3+}$ as shown in (a); (c) high aspect ratio $Gd_2O_3:Eu^{3+}$ nanowires embedded in the matrix of $Gd_2O_3:Eu^{3+}$ nanoflakes obtained after calcination at 750 °C. (d) Schematic diagrams for the structural evolution of the as-synthesised $Gd_2(OH)_3:Eu^{3+}$ and calcined $Gd_2O_3:Eu^{3+}$ nanophosphors

wall carbon nanotubes (MWCNTs) which act as templates (Grandhe *et al*., 2013). Agglomeration of the $Gd_2(OH)_3:Eu^{3+}$ nanoflakes towards micron sized $Gd_2O_3:Eu^{3+}$ flakes also took place after the calcination. The growth of these nanostructures is schematically illustrated in Figure 2 (d).

Figure 3 shows the Tauc plots of the as-synthesised $Gd_2(OH)_3:Eu^{3+}$ and $Gd_2O_3:Eu^{3+}$ powders. The optical band gaps were estimated from the Wood and Tauc relation (Dhananjaya *et al*., 2010) with the indirect allowed electronic transition, n = 2. The indirect band gap herein refers to forbidden electrical dipole transitions which are phonon assisted transitions (Shinde *et al.,* 2012). The straight line segments indicated the optical energy band gap, E_g of 4.95 eV, and 5.31 eV for the as-synthesised $Gd_2(OH)_3:Eu^{3+}$ and $Gd_2O_3:Eu^{3+}$ powders, respectively. The discrepancy of optical band gap between them is due to the different degree of structural order-disorder in their lattices (Krishna *et al*., 2013). As indicated by the larger FWHM of the as-synthesised $Gd_2(OH)_3:Eu^{3+}$ compared to the $Gd_2O_3:Eu^{3+}$, the former has a higher degree of structural defects (Dhananjaya *et al*., 2010). An intermediate energy level can be introduced by the structural defects. This intermediate energy level facilitates a two-step excitation causing a reduction of E_g in $Gd_2(OH)_3:Eu^{3+}$. The as-synthesised hexagonal $Gd_2(OH)_3:Eu^{3+}$ transformed into highly Crystalline cubic $Gd_2O_3:Eu^{3+}$ with fewer defects upon calcination. The hexagonal is compsed of $[Gd(OH)_3]$-clusters connected to each other. Since the The Eu^{3+} dopant is a lattice modifier (Volanti *et al*., 2009), the addition of Eu^{3+} in the hexagonal $Gd(OH)_3$ promotes the expansion of $Gd(OH)_3$ unit cell with high concentration of structural defects (Volanti *et al*., 2009., Omar *et al*., 2016). When the hexagonal $Gd(OH)_3:Eu^{3+}$ is subjected to a calcination, the crystallinity is promoted to form $[GdO_{10}]$ cluster with random dispersion of Eu^{3+} substitution that connected to each other in

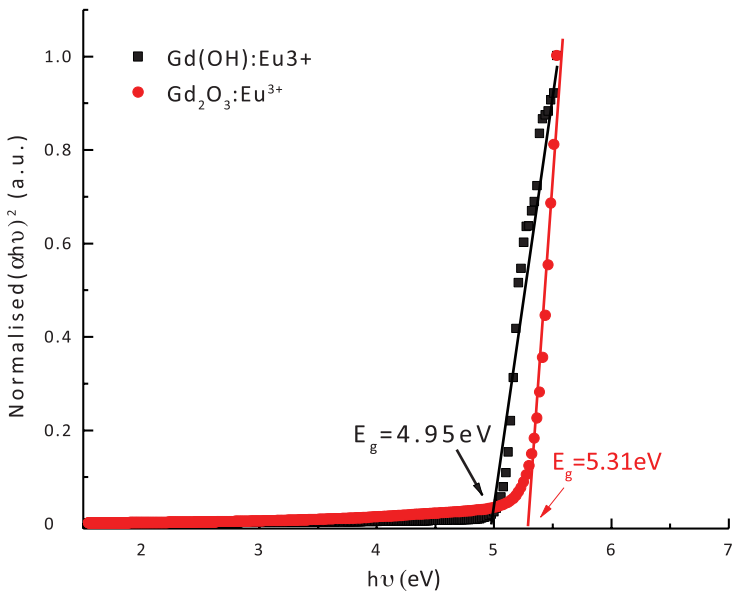


Figure 3: Tauc plots of the as-synthesised $Gd_2(OH)_3:Eu^{3+}$ and $Gd_2O_3:Eu^{3+}$. The optical band gaps of 4.95 eV and 5.31 eV for the $Gd_2(OH)_3:Eu^{3+}$ and $Gd_2O_3:Eu^{3+}$, respectively, were estimated from the Wood and Tauc relation with n = 2 for the indirect allowed electronic transition

compact cubic crystal structure (de Moura *et al*., 2014). The quantity of surface structural defects is reduced as affirmed by the nanostructures evolution mentioned previously. Consequently, the intermediate energy levels within the absorption band of Gd_2O_3:Eu^{3+} is minimized, leading to an increase of E_g.

The photoluminescence (PL) of the $Gd_2(OH)_3$:Eu^{3+} and Gd_2O_3:Eu^{3+} powders were compared to that of the pure Gd_2O_3 and Eu_2O_3. Figure 4 shows the PL emission spectra of these compounds measured in the range of 560-720 nm under the excitation wavelength of 257 nm. This excitation wavelength corresponds to the charge transfer band of Eu^{3+} where the charge is transferred from O^{2-} 2p orbital to Eu^{3+} 4f orbital (Dhananjaya *et al*., 2012). The emission spectra depict the manifolds of Eu^{3+} transitions with $^5D_0$ to ^7F_i transition where i is 1, 2, 3 and 4. For the pure Gd_2O_3, no significant emission was observed from its spectrum. The cubic Gd_2O_3:Eu^{3+} exhibits strong emission at 612 nm with the intensity two times higher than that of the commercially available Eu_2O_3. The peak at 612 nm is responsible for the dominant red emission associated with the $^5D_0$ - $^7F_2$ transition of the Eu^{3+} ions only (Rajan & Gopchandran, 2009; Maalej *et al*., 2015).

Based on the Judd-Ofelt theory (Rajan & Gopchandran, 2009; Shinde *et al*., 2012; Maalej *et al*., 2015), the intensity of $^5D_0 \rightarrow {}^7F_2$ transition is hypersensitive to the symmetry of the surrounding Eu^{3+}. Therefore, the asymmetry ratio, R for $^5D_0 \rightarrow {}^7F_2$ to $^5D_0 \rightarrow {}^7F_1$ transition or $R = \frac{I(^5D_0 \rightarrow {}^7F_2)}{I(^5D_0 \rightarrow {}^7F_1)}$ can be used as a parameter to estimate deviation of the asymmetric coordination polyhedron of Eu^{3+}. The R values for the Gd_2O_3:Eu^{3+}, $Gd_2(OH)_3$:Eu^{3+} and Eu_2O_3 are tabulated in Table 1. The higher R value shown in the cubic Gd_2O_3:Eu^{3+} indicates that majority of Eu^{3+} dopants occupy C_2 sites rather than S_6 (or C_{3i}) sites due to the dominant presence of allowed $^5D_0 \rightarrow {}^7F_2$ electric dipole transition. On the other hand, the hexagonal $Gd_2(OH)_3$:Eu^{3+} and cubic Eu_2O_3 spectra show broader and shifted $^5D_0 \rightarrow {}^7F_1$ and $^5D_0 \rightarrow {}^7F_2$ transition peaks with lower intensities. The lower R values and comparable intensities for both $^5D_0 \rightarrow {}^7F_1$ and $^5D_0 \rightarrow {}^7F_2$ transitions confirm that the occupancy of Eu^{3+} in $Gd_2(OH)_3$ and Eu_2O_3 are relatively random between the C_2 and S_6 sites. The discrepancy of the R values also implies the presence of weaker Eu-O covalent bonding in $Gd_2(OH)_3$:Eu^3 and Eu_2O_3 (Rajan & Gopchandran, 2009).

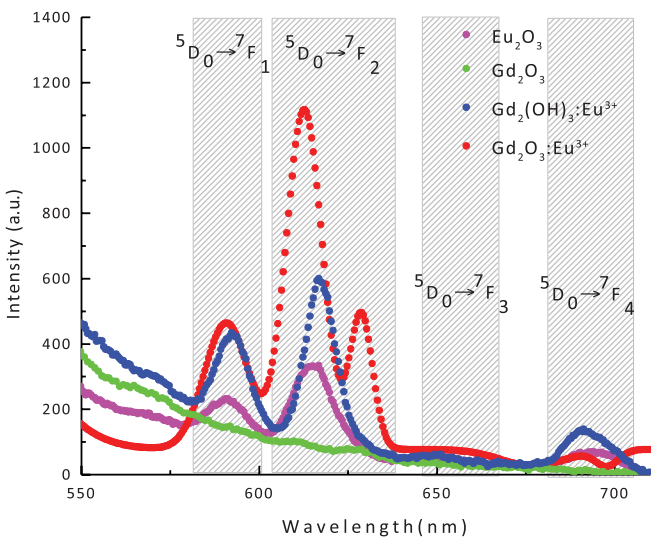


Figure 4: Photoluminescence (PL) emission spectra of the as-synthesised $Gd_2(OH)_3$:Eu^{3+} and calcined Gd_2O_3:Eu^{3+} in comparison to pure Gd_2O_3 and Eu_2O_3. The shaded areas are the emission regions associated with the manifolds of Eu^{3+} with $^5D_0$ to ^7F_i transition where i is 1, 2, 3 and 4

Table 1: Asymmetry ratio, R of $Gd_2O_3:Eu^{3+}$, $Gd_2(OH)_3:Eu^{3+}$ and Eu_2O_3

Compounds	Asymmetric intensity ratio, *R*
$Gd_2O_3:Eu^{3+}$	2.405
$Gd_2(OH)_3:Eu^3$	1.402
Eu_2O_3	1.428

These weak Eu-O bonds act as trapping sites for charge transfer leading to quenching of luminescence. This observation is in fact in good agreement with that found in $Gd_2O_3:Eu^{3+}$ films grown by pulsed laser deposition technique and the $Gd_2O_3:Eu^{3+}$ powders prepared using combustion method (Rajan & Gopchandran, 2009; Dhananjaya *et al*., 2010).

In addition, the results also reveal that the photoluminescence properties are not only rely on the manifold *f-f* transitions of Eu^{3+} dopants but also depend on the crystallographic symmetry and structural imperfection of the Gd_2O_3 host. Owing to the high reflective index and large band gap of Gd_2O_3, the absorption of UV by Gd_2O_3 host lattice is entirely transferred to the Eu^{3+} dopants that are mainly located at the C_2 sites. As a result, a high optical dispersion at 612 nm is induced (Rajan & Gopchandran, 2009). Hence, this profound red emission confirms that Gd_2O_3 is an excellent host which enables efficient energy transfer to the Eu^{3+} dopants.

Conclusion

In summary, this work demonstrates that $Gd_2O_3:Eu^{3+}$ nanowires can be synthesised by means of relatively straightforward hydrothermal route without using any surfactant, catalysts or MWCNTs templates. XRD patterns revealed that the as-synthesised $Gd_2(OH)_3:Eu^{3+}$ evolved from hexagonal structure towards highly crystalline cubic $Gd_2O_3:Eu^{3+}$ after calcination at 750 °C for 5 hours. Simultaneously, the degree of structural order-disorder is reduced leading to the enhancement of band gap of the $Gd_2O_3:Eu^{3+}$ nanophosphors. The $Gd_2O_3:Eu^3$ has a high aspect ratio of 266.7 compared with 6.7 for the as-synthesised $Gd_2(OH)_3:Eu^{3+}$. The combination of symmetric host lattice of Gd_2O_3 and manifold *f-f* transitions of Eu^{3+} stimulate strong red emission associated with $^5D_0 \rightarrow {}^7F_2$ transition at 612 nm. The discrepancy of the *R* values and varied degree of structural imperfections shed some light on the correlation between photoluminescence and structural properties. Hence, controlled growth of nanostructure with high aspect ratio offers a reliable pathway to strongly improve photoluminescence in red region, which is beneficial to biological labelling and optoelectronics.

Acknowledgments

The authors acknowledge the support from the Ministry of Higher Education Malaysia (Research Acculturation Grant Scheme No. 57113). The characterization works conducted in Universiti Putra Malaysia was supported by the Putra Grant No. 9440100.

References

Cullity, B. D., & Stuart, R. S. (2001). *Elements of X-ray diffraction*: Prentice-Hall, Inc.

de Moura, A. P., Oliveira, L. H., Nogueira, I. C., Pereira, P. F., Li, M. S., Longo, E., Varela, J. A., & Rosa, I. L. (2014). Synthesis, structural and photophysical properties of Gd_2O_3: Eu^{3+} nanostructures prepared by a microwave sintering process. *Advances in Chemical Engineering and Science, 4*(03): 374–388.

Dhananjaya, N., Nagabhushana, H., Nagabhushana, B., Chakradhar, R., Shivakumara, C., & Rudraswamy, B. (2010). Synthesis, characterization and photoluminescence properties of Gd_2O_3:Eu^{3+} nanophosphors prepared by solution combustion method. *Physica B: Condensed Matter, 405*(17): 3795-3799.

Dhananjaya, N., Nagabhushana, H., Nagabhushana, B., Rudraswamy, B., Shivakumara, C., & Chakradhar, R. (2012). Spherical and rod-like Gd_2O_3: Eu^{3+} nanophosphors—Structural and luminescent properties. *Bulletin of Materials Science, 35*(4): 519-527.

Goldys, E. M., Drozdowicz-Tomsia, K., Jinjun, S., Dosev, D., Kennedy, I. M., Yatsunenko, S., & Godlewski, M. (2006). Optical characterization of Eu-doped and undoped Gd_2O_3 nanoparticles synthesized by the hydrogen flame pyrolysis method. *Journal of the American Chemical Society, 128*(45): 14498-14505.

Grandhe, B. K., Bandi, V. R., Jang, K., Kim, S. S., Shin, D.-S., Lee, Y., Lin, J., & Song, T. (2013). Synthesis and characterization of Eu^{3+} doped Gd_2O_3 nanotubes using multi wall carbon nanotubes as removable templates. *Metals and Materials International, 19*(3): 507-511.

Guo, H., Yang, X., Xiao, T., Zhang, W., Lou, L., & Mugnier, J. (2004). Structure and optical properties of sol–gel derived Gd_2O_3 waveguide films. *Applied Surface Science, 230*(1): 215-221.

Hazarika, S., & Mohanta, D. (2016). Oriented attachment (OA) mediated characteristic growth of Gd_2O_3 nanorods from nanoparticle seeds. *Journal of Rare Earths, 34*(2): 158-165.

Jeong, J. H., Yang, H. K., Moon, B. K., Bae, J. S., Yi, S., Choi, H., Kim, J. H., & Chung, S. T. (2006). Li-doping effect on enhancement of photoluminescence in Gd_2O_3: Eu^{3+} films. *Optical Materials, 28*(6): 693-697.

Kharisov, B. I., Kharissova, O. V., & Méndez, U. O. (2012). *Microwave hydrothermal and solvothermal processing of materials and compounds*: INTECH Open Access Publisher.

Kiraly, B., Yang, S., & Huang, T. J. (2013). Multifunctional porous silicon nanopillar arrays: antireflection, superhydrophobicity, photoluminescence, and surface-enhanced Raman scattering. *Nanotechnology, 24*(24): 245704.

Krishna, R. H., Nagabhushana, B., Nagabhushana, H., Murthy, N. S., Sharma, S., Shivakumara, C., & Chakradhar, R. (2013). Effect of calcination temperature on structural, photoluminescence, and thermoluminescence properties of Y_2O_3: Eu^{3+} nanophosphor. *The Journal of Physical Chemistry C, 117*(4): 1915-1924.

Lee, K.-H., Bae, Y.-J., & Byeon, S.-H. (2008). Nanostructures and photoluminescence properties of Gd_2O_3: Eu red-phosphor prepared via hydrothermal route. *Bulletin of the Korean Chemical Society, 29*(11): 2161.

Lee, K.-H., Lee, B.-I., You, J.-H., & Byeon, S.-H. (2010). Transparent Gd_2O_3: Eu phosphor layer derived from exfoliated layered gadolinium hydroxide nanosheets. *Chemical Communication, 46*(9): 1461-1463.

Lin, C.-C., Lin, K.-M., & Li, Y.-Y. (2007). Sol–gel synthesis and photoluminescent characteristics of Eu^{3+}-doped Gd_2O_3 nanophosphors. *Journal of luminescence, 126*(2): 795-799.

Luo, N., Yang, C., Tian, X., Xiao, J., Liu, J., Chen, F., Zhang, D., Xu, D., Zhang, Y., Yang, G., Chen, D., & Li, L. (2014). A

general top-down approach to synthesize rare earth doped-Gd_2O_3 nanocrystals as dualmodal contrast agents. *Journal of Materials Chemistry B, 2*(35): 5891-5897.

Maalej, N. M., Qurashi, A., Assadi, A. A., Maalej, R., Shaikh, M. N., Ilyas, M., & Gondal, M. A. (2015). Synthesis of Gd_2O_3: Eu nanoplatelets for MRI and fluorescence imaging. *Nanoscale research letters, 10*(1): 1-10.

Mukherjee, S., Sudarsan, V., Vatsa, R., & Tyagi, A. (2009). Luminescence studies on lanthanide ions (Eu^{3+}, Dy^{3+} and Tb^{3+}) doped YAG:Ce nano-phosphors. *Journal of luminescence, 129*(1): 69-72.

Omar, N. A. S., Fen, Y. W., Matori, K. A., Zaid, M. H. M., Norhafizah, M. R., Nurzilla, M., & Zamratul, M. I. M. (2016). Synthesis and optical properties of europium doped zinc silicate prepared using low cost solid state reaction method. *Journal of Materials Science: Materials in Electronics*, *27*(2): 1092-1099.

Rajan, G., & Gopchandran, K. G (2009a). Enhanced luminescence from spontaneously ordered Gd_2O_3:Eu^{3+} based nanostructures. *Applied Surface Science, 255*(22): 9112-9123.

Rajan, G., & Gopchandran, K. G (2009b). Engineering of luminescence from Gd_2O_3:Eu^{3+} nanophosphors by pulsed laser deposition. *Optical Materials, 32*(1), 121-132. doi: http://dx.doi.org/10.1016/j.optmat.2009.06.017.

Shim, K., Yang, H., Moon, B., Jeong, J., Yi, S., & Kim, K. (2007). Improved photoluminescence of pulsed-laser-ablated $Y_{1-x}Gd_xVO_4$: Eu^{3+} thin film phosphors by Gd substitution. *Applied Physics A, 88*(4): 623-626.

Shin, S. H., Kang, J. H., Jeon, D. Y., & Zang, D. S. (2005). Enhancement of cathodoluminescence intensities of Y_2O_3: Eu and Gd_2O_3: Eu phosphors by incorporation of Li ions. *Journal of luminescence, 114*(3): 275-280.

Shinde, K. N., Dhoble, S. J., Swart, H. C., & Park, K. (2012). *Phosphate Phosphors for Solid-State Lighting*. Berlin, Heidelberg: Springer Berlin Heidelberg.

Telgmann, L., Sperling, M., & Karst, U. (2013). Determination of gadolinium-based MRI contrast agents in biological and environmental samples: A review. *Analytica Chimica Acta, 764*: 1-16. doi: http://dx.doi.org/10.1016/j.aca.2012.12.007.

Volanti, D. P., Rosa, I. L., Paris, E. C., Paskocimas, C. A., Pizani, P. S., Varela, J. A., & Longo, E. (2009). The role of the Eu^{3+} ions in structure and photoluminescence properties of $SrBi_2Nb_2O_9$ powders. *Optical Materials*, *31*(6): 995-999.

Yang, H., Lee, H., & Holloway, P. H. (2005). Anisotropic growth of luminescent Eu^{3+}-or Er^{3+}-doped Gd_2O_3 nanocrystals. *Nanotechnology, 16*(12): 2794.

Yang, J., Li, C., Cheng, Z., Zhang, X., Quan, Z., Zhang, C., & Lin, J. (2007). Size-tailored synthesis and luminescent properties of one-dimensional Gd_2O_3: Eu^{3+} nanorods and microrods. *The Journal of Physical Chemistry C, 111*(49): 18148-18154.